Author/s:
Ramdzan, YM;Polling, S;Chia, CPZ;Ng, IHW;Ormsby, AR;Croft, NP;Purcell, AW;Bogoyevitch, MA;Ng, DCH;Gleeson, PA;Hatters, DM

Title:
Tracking protein aggregation and mislocalization in cells with flow cytometry

Date:
2012-01-01

Citation:
Ramdzan, Y. M., Polling, S., Chia, C. P. Z., Ng, I. H. W., Ormsby, A. R., Croft, N. P., Purcell, A. W., Bogoyevitch, M. A., Ng, D. C. H., Gleeson, P. A. & Hatters, D. M. (2012). Tracking protein aggregation and mislocalization in cells with flow cytometry. Nature Methods, 9 (5), pp.467-470. https://doi.org/10.1038/nmeth.1930.

Tracking protein aggregation and mislocalization in cells with flow cytometry

Yasmin M. Ramdzan[1], Saskia Polling[1], Cheryl P. Z. Chia[1], Ivan H. W. Ng[1,2], Angelique R. Ormsby[1], Nathan P. Croft[1], Anthony W. Purcell[1], Marie A. Bogoyevitch[1], Dominic C. H. Ng[1], Paul A. Gleeson[1] and Danny M. Hatters[1,*]

[1]Department of Biochemistry and Molecular Biology and Bio21 Molecular Science and Biotechnology Institute. 30 Flemington Road. The University of Melbourne. Melbourne VIC 3010 Australia

[2]Department of Biochemistry and Molecular Biology, Monash University, Clayton Victoria 3800, Australia

[*]Corresponding author
Ph: +61 3 8344 2530
Fax: +61 3 9348 1421
Email: dhatters@unimelb.edu.au

Abstract:

We apply pulse shape analysis (PulSA) to monitor protein localization changes in mammalian cells by flow cytometry. PulSA enabled high-throughput tracking of protein aggregation as well as translocation from the cytoplasm to the nucleus, trafficking from the plasma membrane to the Golgi, and stress granule formation. Combining PulSA with tetracysteine-based oligomer sensors in a cell model of Huntington's disease enabled further separation of cells enriched with monomers, oligomers and inclusions.

The mislocalization of proteins or their aggregation into abnormal cellular puncta is a hallmark of many human diseases, including Alzheimer's, Parkinson's, amyotrophic lateral sclerosis and Huntington's. Yet, defining how aggregation relates to toxicity or cellular dysfunction remains a difficult challenge because of a dearth of approaches that can systematically examine different sized protein aggregates *in situ* and relate their presence to specific biological outcomes [1]. This

is particularly relevant in light of increasing evidence suggesting that smaller, nanometer-sized aggregate forms called oligomers are more toxic than larger ones for many aggregating proteins [2, 3]. In addition, cells actively sort misfolded proteins into punctate reservoirs such as aggresomes or inclusions to protect themselves from toxicity caused by dispersed forms of the misfolded proteins [4-6]. Hence the development of new assays and procedures that can independently track different aggregated forms of proteins in intact cells would be invaluable for relating different stages of aggregation to specific biological outcomes or testing the efficacy of therapeutic agents that target specific aggregated forms.

Standard approaches for detecting aggregates involve microscopy-based methods which pose challenges for high throughput and quantitative analysis. High content screening approaches in a microscopy format have partially addressed the throughput and quantitative challenges, but are still restricted in their capability for segmentation and feature extraction – especially in highly clustered cells - and typically require complex data analysis algorithms, background corrections and specialized instrumentation and cannot recover distinct populations for further analysis [7]. Furthermore the acquisition of two-dimensional images creates large data files and necessitates complex data analysis strategies.

Our initial objective was to develop a fast, simple and quantitative method to separate cells expressing mutant polyglutamine (polyQ)-expanded huntingtin, which causes Huntington's disease [8], that had shifted from a diffuse cytosolic distribution into punctate micrometer-sized inclusions. Pulse shape analysis (PulSA) by flow cytometry has been used previously to analyze particles of different size or sort cells with different-sized organelles [9]. We reasoned that it should be possible to similarly use pulse width and height measurements of fluorescently labeled proteins to distinguish protein localization differences in cells (**Fig. 1a**). Flow cytometry of mouse neuroblastoma (Neuro2a) cells transfected with the exon 1 fragment of Htt (Htt_{ex1}) fused to the GFP variant Emerald showed that aggregation-prone mutants of Htt_{ex1}-Emerald (with polyQ lengths 46 and 72) formed a new subpopulation relative to the non-aggregating 25Q form of Htt_{ex1}-Emerald (**Fig. 1b**). This subpopulation (i) had a narrower and higher pulse shape than the other population of cells (ni), which is consistent with the protein localized into denser, more compact structures, characteristic of inclusions. Examination of the width and height histograms of the whole population further illustrates a shift in the population to higher pulse heights and

narrower pulse widths (**Fig. 1c**). Assessment of the i and ni populations by microscopy confirmed that the ni population included cytosolically distributed diffuse Htt only, whereas the i population contained cells each with inclusions (**Fig. 1d**). Similar results were also obtained using untagged Htt exon 1 detected with antibodies or by replacing the GFP with a small six amino acid tag (**Supplementary Fig. 1**). PulSA also measured changes in numbers of cells with inclusions using known modulators of inclusion formation: chaperones Hsp40/Hsp70 overexpression to suppress inclusion formation (**Supplementary Fig. 2a**) and the proteasome inhibitor, MG132, to increase inclusion formation (**Supplementary Fig. 2b**). .

To examine whether PulSA can be applied to studying other proteins known to mislocalize in disease, we examined Neuro2a cells expressing superoxide dismutase 1 (SOD1). SOD1 is normally diffusely distributed throughout the cell whereas an SOD1 mutant leading to amyotrophic lateral sclerosis (A4V substitution) forms abnormal cytoplasmic puncta [10]. Wild-type SOD1-GFP revealed a single population analogous to the ni population of Htt_{ex1}-GFP (**Supplementary Fig. 3a**). In contrast, the A4V SOD1-GFP mutant formed a subpopulation with a narrower pulse width (i population). The i population had punctate SOD1-GFP in 98.4 % of sorted and recovered cells when assayed by microscopy (n = 248), which compared to 7.3 % in the unsorted population (n = 247; z-test $P < 0.001$), whereas 1.0% of the cells in the ni population had inclusions (n = 487; P = 0.006) (**Supplementary Fig. 3b).** The high efficiency of the separation occurred despite the apparent significant overlap in the gating strategy for the ni and i populations when the wild-type SOD1 ni population was used to calibrate the mutant SOD1 ni population (**Supplementary Fig. 3b).** This result likely arises from the reduced expression levels of the A4V shifting the boundary position dividing i and ni, and hence suggests the i gate boundary must considered in context of the overall symmetry of the width and height distributions of the cells when using a 2-dimensional gating strategy (**Supplementary Fig. 3c**).

We next assessed the applicability of PulSA for monitoring protein localization differences in three other biological processes. We first investigated the internalization and trafficking of plasma membrane-bound protein to the Golgi using Shiga toxin B (STxB) (**Fig. 1e**). StxB was labeled with amine-reactive Cy3 and applied to HeLa cells on ice to enable binding of the toxin under conditions non-permissive for endocytosis. After1 h treatment at 37 ^{o}C, PulSA showed a shift in localization from the plasma membrane to the Golgi by microscopy, which corresponded

to a large and significant decrease in pulse width values compared to cells fixed immediately after StxB binding (**Fig. 1e** and **Supplementary Fig. 4a**). To examine whether the change in pulse width was specific for StxB relocalization, we also labeled the nucleus with DAPI and the Golgi by immunofluorescence (for Golgi resident GM130) for concurrent PulSA. These two organelles showed minimal changes in pulse width, validating the sensitivity of PulSA in monitoring protein translocation from the plasma membrane to the Golgi (**Fig. 1e**). We also investigated the formation of cytosolic stress granules by HuR (**Fig. 1f**). Endogenous HuR in HeLa cells was monitored by immunofluorescence, and normally resided predominately in the nucleus (**Fig. 1f** and **Supplementary Fig. 4b**). Treatment of the cells with the stressor arsenite for 60 min led to HuR forming many cytoplasmic puncta, which correlated with an increase in the pulse width values by PulSA (**Fig. 1f** and **Supplementary Fig. 4b**). The control staining of the nucleus with DAPI showed no change in pulse width values, confirming the sensitivity of PulSA for following protein relocalization within the cells (**Fig. 1f)**. Our last biological process to be tracked by PuLSA was the translocation of the transcription factor Stat3 from the cytoplasm to the nucleus upon cytokine stimulation with oncostatin M (**Fig. 1g**). Stat3 was detected with immunofluorescence and monitored for nuclear localization by microscopy after 15 min stimulation (**Fig 1g**). There was a sharp decrease in the PulSA width corresponding to nuclear localized Stat3 compared to cytoplasmic Stat3 in the untreated cells, and a minimal change for the nucleus (stained with Hoechst 33342). Hence for each of our three test cases, the pulse width of the target protein shifted to match its cellular location as assessed by confocal microscopy (either attached on the plate –**Fig. 1e-g** or in suspension - **Supplementary Fig. 4a-c**). These experiments showed that PulSA can track protein localization differences of endogenous proteins detected with immunolabelling – and hence should be useful in studying protein translocation in a wide range of contexts.

We examined whether we could gain additional insight to the transitions of polyQ-expanded Htt from monomers to oligomers and inclusions in individual cells by combining PulSA with our previously developed tetracysteine (TC) sensors of Htt_{ex1} that discriminate between mutant Htt_{ex1} monomers and submicroscopic oligomers [11]. In the TC1 Htt_{ex1} sensor, the TC motif is inserted into a region of the Htt sequence that binds FlAsH irrespective of whether Htt_{ex1} is monomeric or oligomeric [11]. However, in the TC9 sensor, the TC motif is inserted in a region whereby it only binds FlAsH when Htt_{ex1} is monomeric—and in all oligomers binding is

completely impeded [11]. The colocalization of the Cerulean fluorescent protein tag, which tracks Htt_{ex1} protein, with TC9 FlAsH reactivity enables the extent of monomers to be determined by correlation of Cerulean fluorescence with FlAsH reactivity [11] (**Supplementary Fig. 5**). We have previously used the TC sensors to show that 46Q- Htt_{ex1} forms submicroscopic oligomers located diffusely throughout the cytosol of a subset of Neuro2a cells [11]. Yet, it remains unclear how oligomers form within cells in a time and Htt_{ex1}-concentration dependent manner.

We first validated the use of the TC sensors in a flow cytometry format. Using the TC1 sensor we saw no major differences in the populations of cells binding FlAsH when we compared 25Q and 46Q forms (High-FlAsH reactive (HFR) and poor-FlAsH reactive populations (PFR)) (**Fig. 2a**). TC9 on the other hand, revealed a substantial population of cells showing poor-FlAsH-reactivity when in the 46Q form (**Fig. 2a**). When reanalyzing the data by PulSA we saw that the majority of the cells contained in the PFR population of 46Q expressing cells detected with the TC9 sensor were contained in the i population, indicating that most of the aggregated Htt_{ex1} resided in inclusions (**Fig. 2b**).

These results thus indicated a strategy to combine PulSA with TC9 reactivity to separate cells into three groups: those enriched in monomers (HFR/ni); those enriched in oligomers but without inclusions (PFR/ni); and those with inclusions (PFR/i) (**Fig. 2c**). Cells expressing the TC9 sensor forms of 25Q or 46Q Htt_{ex1}-CFP were stratified into three different expression levels at 3 different days after transfection (**Fig. 2d**) and analysed by TC9 reactivity and PulSA (**Fig. 2e, f**). The PFR/i population was most abundant at higher Htt_{ex1} expression levels and increased in proportion over time (**Fig. 2e**). Indeed, the highest-expressing population tier had more than 80 % of its cells in the PFR/i subpopulation by day 3, whereas the lowest expressing tier had only 1 % of its cells in the PFR/i subpopulation, indicating expression levels profoundly dictate the risk of cells forming inclusions (**Fig. 2e**). By contrast, the PFR/ni population was most abundant in the medium and lowest Htt_{ex1}-expression population tiers (**Fig. 2f**). Interestingly, there were negligible PFR/ni cells in the highest-expression tier – even at early time points – which could indicate conversion of oligomers to inclusions is faster at higher cellular Htt_{ex1} concentrations. Alternatively, inclusions could form concurrently with oligomers, which would not be detectable with these methods. Collectively, these data showed the potential of the pulse-shape method for gaining new insight to kinetic or cellular parameters driving Htt aggregation

and inclusion formation of each cell in whole cell populations. The data we have here are consistent with a model in which oligomers form prior to inclusions, building upon recent microscopy approaches at the individual cell level [11-13] (**Supplementary Fig. 6** and **Supplementary Note 1**).

In summary, PulSA provides a powerful and simple method for extracting protein localization differences in cells. The major features of the method are the simplicity, quantitative nature, high throughput and capacity to examine cells with different protein expression levels or to examine protein localization in combination with other markers, such as viability, apoptosis or gene co-expression. The method is complemented by recent developments in one-dimensional confocal microscopy equipped with multichannel flow lines that, similarly to PulSA, provides information about the shape patterns in cells [14]. An attractive feature of the PulSA method is its use of standard flow cytometry instrumentation and straightforward data analysis.

Acknowledgements

This work was funded by grants to D.M.H. (NHMRC project grant 566640). D.M.H. is a Grimwade Fellow, supported by the Miegunyah Trust. D.C.H.N. is a CR Roper Fellow. The SOD1-GFP fusion constructs were provided by B. J. Turner, from the Florey Neurosciences Institute, Australia. *HSPA1A* (Hsp70) and *DNAJB1* (Hsp40) in the pCMV vector was provided by P. Muchowski from the Gladstone Institute of Neurological Disease and University of California, San Francisco.

Author Contributions

Y.M.R., S.P., C.P.Z.C., I.H.W.N., N.P.C., A.W.P., D.C.H.N. and A.R.O. performed experiments and/or helped interpret the data. Y.M.R., M.A.B., D.C.H.N. and P.A.G. contributed in the design some of the experiments. D.M.H. conceived of the method, oversaw implementation of the experiments and wrote the manuscript.

Competing financial interests

The authors declare no competing financial interests.

Figure legends

Figure 1. Use of PulSA to track changes in protein localization in cells. (**a**) Principle behind pulse shape analysis (PulSA). (**b**) Cytograms showing pulse width versus height of Htt_{ex1}-Emerald of subpathogenic (25Q) and pathogenic (46Q and 72Q) variants when transfected into Neuro2a cells. Two distinct populations are distinguished: ni – cells with diffuse Htt distributions and i – cells with inclusions. **c**) Data reanalyzed as histograms for width (left) and height (right) and also including the 97Q variant. For clarity, each sample is offset on the y axis by 0.5 units for the height histogram and 1 unit for the width histogram. The median values are shown above graphs for statistical comparisons (n = 3, ± s.d. shown. ANOVA). **d)** Verification of ni and i populations by microscopy after the cells were sorted and recovered from the flow cytometer (they were analyzed when fixed). **(e-g)** Application of PulSA to monitor three different biological processes. (**e**) Endocytosis from the plasma membrane to the Golgi organelle. Cy3-labeled Shiga toxin B (STxB) was added to HeLa cells on ice, which binds to the plasma membrane (t = 0) and is then trafficked to the Golgi (t = 60 min at 37 ^{o}C). (**f**) Stress granule formation. Tracking of the endogenous protein HuR, detected with immunofluorescence, before and after 1 h exposure to stress induced by arsenite treatment. (**g**) Cytokine-stimulated nuclear translocation. Tracking of endogenous Stat3 by immunofluorescence before or after 15 min cytokine Oncostatin M treatment. Each **e-g** panel shows images of the adherent HeLa cells before and after treatment or at two different time points. The cells are labeled with dyes to track the nucleus or the Golgi organelle. To the right, the pulse width histograms and the median pulse widths for the dyes or the tracked protein (n = 3 independent experiments; ± s.d. shown).

Figure 2. PulSA combined with TC sensors of Htt oligomerization selectively separate cells enriched in Htt monomers, oligomers or inclusions. (**a**) Flow cytometry analysis of live Neuro2a cells expressing the TC9 sensor (24 hours after transfection) in the 25Q and 46Q, after labeling with FlAsH. (**b**) Simultaneous PulSA (on Cerulean fluorescence) of cells expressing the TC1 or TC9 reporter and transfected with 25Q or 46Q forms of Htt. The PFR population is shown in red, the HFR in blue, and untransfected cells in black. (The non-aggregating 25Q forms do not form an i population, but this gate provides a useful reference for bleed through.) (**c**) Schematic describing how PulSA and TC sensors can separate cells into three groups. (**d**)

Classification of cells expressing the TC9 reporters based on expression levels of Htt (Cerulean fluorescence). Shown is one replicate of three of the 25Q TC9 at 3 days expression. (**e**) and (**f**) Tracking of populations of cells classified according to **(d)** over time. with inclusions **(**PFR/i; panel **e**) and enriched with oligomers but no inclusion (PFR/ni; panel **f**) over time after transfection. $n = 3$ independent experiments, mean ± s.d. shown. *P* values less than 0.05 shown for clarity.

Methods

Cloning of constructs

For the TC sensor experiments, Htt_{ex1} cDNA was cloned into a pcDNA3.2 vector (Life Technologies) with a C-terminal fusion to the fluorescent protein Cerulean, which is a variant of the cyan fluorescent protein [15], as previously described [11]. The TC1 and TC9 variants were generated as described [11]. The Htt_{ex1}-Emerald constructs in the pT-Rex vector backbone (Life Technologies) were produced as described [16]. For the Htt_{ex1} with a C-terminal TC tag instead of the GFP, PCR-mediated standard cloning procedures were performed to generate the following C-terminal sequence of Htt exon 1, with the Htt exon 1 sequence underlined: HRPCCPGCCGSENLYFQ*. GFP^{inv} comprises the Emerald fluorescent protein with the Y66L mutation to prevent formation of the fluorophore and was prepared in the pcDNA3.2 vector as described previously [16].

General cell culture

Neuro-2a cells were maintained in OptiMem (Life Technologies) supplemented with 10 % fetal calf serum, 1 mM glutamine, 100 U/ml penicillin, and 100 µg/ml streptomycin in a humidified incubator with 5 % atmospheric CO_2. HeLa and HEK293 cells were maintained in DMEM (Life Technologies) supplemented with 10 % fetal calf serum, 1 mM glutamine, 100 U/ml penicillin, and 100 µg/ml streptomycin in a humidified incubator with 5 % atmospheric CO_2.

FlAsH staining

2×10^5 cells were plated in individual wells of a 24-well tissue culture plate. The following day the cells in each well were transfected with 2 µl Lipofectamine 2000/0.8 µg vector DNA according to the manufacturer's instructions (Life Technologies). The next day, the media was

changed (500 µl), and for the time course, changed daily thereafter. Before harvesting, cells were labeled on the plate with FlAsH (Life Technologies). First, cells were rinsed twice with 500 µl of pre-warmed Hank's buffered salt solution (HBSS) buffer (Life Technologies), and labelled for 30 min with 500 µl pre-warmed HBSS containing 1 µM FlAsH and 10 µM EDT at 37 ºC. The cells were washed in 500 µl pre-warmed HBSS containing 250 µM dimercaptopropanol (BAL) for 15 min, and the solution was replaced with pre-warmed HBSS. The cells were lifted in 500 µl phosphate buffered saline (PBS) by gentle pipetting. Cell suspensions were kept on ice until analysis by flow cytometry (which was all completed within 1 h after labeling).

Cell preparation for sorting and imaging

1×10^6 cells were plated in individual wells of a 6-well tissue culture plate. The following day the cells in each well were transfected with 10 µl Lipofectamine 2000/4 µg vector DNA according to the manufacturer's instructions (Life Technologies). After 6 h, the media was changed (2 ml). For SOD1-GFP, cells were harvested 24 h post transfection. For Htt_{ex1}-Emerald, the media was replaced again 24 h post transfection. Cells were harvested at 48 h post transfection by first rinsing in PBS, followed by resuspension in PBS with a cell scraper and gentle pipetting. Cells were pelleted (1,600 *g*; 3 min) and resuspended in 2 ml 2% (v/v) paraformaldehyde for 30 min at room temperature. Cells were again pelleted (1,600 *g*; 3 min), resuspended in 2 ml PBS and filtered through 100 micron nylon mesh before analysis by flow cytometry.

Flow cytometry and confocal microscopy

Cells were analysed at a medium flow rate in an LSRFortessa flow cytometer, equipped with 405 nm, 488 nm, 561 nm and 640 nm lasers (BD Biosciences). 50-100,000 events were collected, using a forward scatter threshold of 5,000. Data were collected in pulse height, area and width parameters for each channel. For Cerulean, DAPI and Hoechst 33342, data were collected with the 405 nm laser 450/50 nm bandpass filter. For FlAsH, AlexaFluor 488, and GFP, data were collected with the 488 nm laser 530/30 nm bandpass filter. For Cy3, data were collected with the 561 nm laser and 610/20 bandpass filter.

For cell sorting and subsequent imaging by microscopy, cells were collected directly into an 8 well µ–slide (Ibidi) by a FACSAria cell sorter, equipped with a 488 nm laser line (BD

Biosciences). These cells were imaged by confocal microscopy using a HC PL APO lbd.BL 20.0×0.70 IMM objective (Leica LCS SP2 confocal imaging system). For the imaging of other unfractionated cells, single cell suspensions of fixed cells were dropped on a glass slide, followed by sealing with a coverslip and varnish. All adherent cells and suspension cells were imaged with the 100×1.4 NA HCX PL APOCS oil immersion objective. Images of multicolour labelled samples were acquired sequentially.

Flow cytometry data were analysed with FACSDiva software (BD Biosciences). For histogram analysis, FCS data was exported into text format using FCS Extract 1.02 software (Earl F Glynn, Stowers Institute for Medical Research) and analysed in Microsoft Excel.

Shiga toxin B experiments

STxB was purified as described [17] and labeled with Cy3 using an amine-reactive conjugation kit (PA23001; GE Healthcare). The internalization assay for Cy3-labelled Shiga toxin B fragment (Cy3-STxB) was performed as described previously for adherent HeLa cells [18] and modified as followed for cells in suspension and subsequent flow cytometry. Briefly, HeLa cells were trypsinized and washed twice with PBS. Cells were resuspended in Cy3-STxB diluted to 1 µg/ml in cold serum-free DMEM, and incubated on ice for 30 min. Cells were washed twice and either fixed in a final concentration of 2 % paraformaldehyde (PFA), or incubated at 37 ºC for 1 h in warm serum-free media before PFA fixation. Cells were permeabilized in 0.1 % (w/v) Triton X100/PBS for 15 min and blocked in 10 % (w/v) fetal calf serum in PBS for 30 min. Single cell suspensions were washed with 0.1 % (w/v) Tween 20/PBS and stained with mouse anti-GM130 antibody (#610822, BD Biosciences) followed by AlexaFluor488-conjugated anti mouse IgG (Life Sciences), to mark the Golgi compartment. Washes were carried out using 0.1 % (w/v) Tween 20/PBS in between staining with primary and secondary antibodies. Nuclei were stained with 4′,6-Diamidino-2-phenylindole dihydrochloride (DAPI). Cells were resuspended in 1 % (w/v) BSA in PBS prior to flow cytometry. For the imaging of adherent cells, cells were grown, treated and fixed on coverslips (or in µ-slides) and immunolabeled using the antibody steps described above.

HuR experiments

HeLa cells were plated at a density of 2.5×10^6 cells on a 10 cm plate. The next day, cells were treated with 350 µM arsenite for 60 min. The cells were washed in PBS, trypsinized and fixed in 4 % PFA (v/v) for 30 min. The cells were washed in PBS, permeabilized in 0.2 % (v/v) Triton X100/PBS for 20 min, blocked in 10 % (v/v) fetal calf serum in 0.1 % (v/v) Tween 20/PBS for 25 min and stained with primary mouse anti HuR antibody (SC-5261; Santa Cruz Biotechnology) in 0.1 % (w/v) BSA/PBS for 1.5 h. The cells were washed twice with 0.1 % (v/v) Tween 20/PBS and then stained with Cy3-conjugated anti-mouse IgG in 0.1 % (w/v) BSA/PBS for 1.5 h. Nuclei were stained with Hoechst 33342 at room temperature for 15 min. Washes were carried out and cells were resuspended in PBS prior to flow cytometry. For the imaging of adherent cells, cells were grown, treated, fixed and immunolabeled on coverslips (or in µ-slides) using the steps described above, except for trypsinization.

Stat3 experiments

HeLa cells were plated at a density of 2.5×10^6 cells on a 10 cm plate. The next day, the media was changed with DMEM and1 mM glutamine, 100 U/ml penicillin, and 100 µg/ml streptomycin and the cells grown a further 16 h. The cells were trypsinized and treated with 10 ng/mL Oncostatin M (#496260, Merck) for 15 min followed by a wash in PBS before fixation in 4 % (v/v) PFA for 30 min. The cells were washed in PBS, permeabilized in 0.2 % (v/v) Triton X100/PBS for 20 min, blocked in 10 % (v/v) fetal calf serum in 0.1 % (v/v) Tween 20/PBS for 25 min and stained with primary rabbit anti-Stat3 c20 antibody (SC-482; Santa Cruz Biotechnology) in 0.1 % (w/v) BSA/PBS for 1.5 h. The cells were washed twice with 0.1 % (v/v) Tween 20/PBS and then stained with AlexaFluor488-conjugated anti rabbit IgG in 0.1 % (w/v) BSA/PBS for 1.5 h. Nuclei were stained with Hoechst 33342 at room temperature for 15 min. Washes were carried out and cells were resuspended in PBS prior to flow cytometry. For the imaging of adherent cells, cells were grown, treated, fixed and immunolabeled on coverslips (or in µ-slides) using the steps described above, except for trypsinization.

Chaperone and MG132 experiments

1×10^6 cells (Neuro2a for the chaperone experiments and HEK293 for the MG132) were plated in individual wells of a 6-well tissue culture plate. For the MG132 experiments, the cells were transfected with 10 µl Lipofectamine 2000/4 µg Htt-Emerald vector according to the

manufacturer's instructions (Life Technologies) the following day. For the chaperone experiments three vectors were combined to a total of 4 µg of DNA with the Htt and chaperones each contributing 1.33 µg DNA The remaining quantity of DNA was made up with GFP^{inv}. 6 h after transfection the media was refreshed. For the MG132 experiments, MG132 was added to the cells 24 h after transfection at a concentration of 50 µM. 48 h after transfection cells were rinsed in PBS, and lifted in PBS with a cell scraper and gentle pipetting, pelleted and resuspended in 2 ml 2 % (v/v) paraformaldehyde for 30 min at room temperature. The cells were pelleted, resuspended in 2 ml PBS and filtered through 100 micron nylon mesh before analysis by flow cytometry.

For Western blots, Htt-Emerald and GFP^{inv} were detected using an anti-GFP antibody (A6455; Life Technologies). Hsp40 and Hsp70 were detected with mouse anti-DNAJB1 (TA502195; Origene) and mouse anti HSPA1A (TA500772; Origene) antibodies respectively.

Statistical analysis

Statistical analyses were performed using the Sigmaplot 12 software package (Systat). For evaluation of differences in means (and standard deviations) the two-tailed Student's t-test was used for two-sample comparisons and ANOVA was used for multiple comparisons. Differences in proportions were evaluated using the z-test with the Yates correction.

References

1. Hatters, D.M. Protein Misfolding Inside Cells: The Case of Huntingtin and Huntington's Disease. *IUBMB Life* **60**, 724-728 (2008).
2. Silveira, J.R. et al. The Most Infectious Prion Protein Particles. *Nature* **437**, 257-261 (2005).
3. Bucciantini, M. et al. Inherent Toxicity of Aggregates Implies a Common Mechanism for Protein Misfolding Diseases. *Nature* **416**, 507–511 (2002).
4. Arrasate, M., Mitra, S., Schweitzer, E.S., Segal, M.R. & Finkbeiner, S. Inclusion Body Formation Reduces Levels of Mutant Huntingtin and the Risk of Neuronal Death. *Nature* **431**, 805-810 (2004).
5. Johnston, J.A., Ward, C.L. & Kopito, R.R. Aggresomes: a cellular response to misfolded proteins. *J. Cell Biol.* **143**, 1883-1898 (1998).
6. Kaganovich, D., Kopito, R. & Frydman, J. Misfolded Proteins Partition Between Two Distinct Quality Control Compartments. *Nature* **454**, 1088-1095 (2008).
7. De Vos, W.H., Van Neste, L., Dieriks, B., Joss, G.H. & Van Oostveldt, P. High content image cytometry in the context of subnuclear organization. *Cytometry Part A* **77A**, 64-75 (2010).
8. MacDonald, M.E. et al. A Novel Gene Containing a Trinucleotide Repeat that is Expanded and Unstable on Huntington's Disease Chromosomes. *Cell* **72**, 971-983 (1993).
9. Hoffman, R.A. Pulse width for particle sizing. *Curr. Protoc. Cytom.* **Chapter 1**, 1.23.21-21.23.17 (2009).
10. Deng, H.X. et al. Amyotrophic lateral sclerosis and structural defects in Cu,Zn superoxide dismutase. *Science* **261**, 1047-1051 (1993).
11. Ramdzan, Y.M. et al. Conformation sensors that distinguish monomeric proteins from oligomers in live cells. *Chem. Biol.* **17**, 371-379 (2010).
12. Ossato, G. et al. A Two-Step Path to Inclusion Formation of Huntingtin Peptides Revealed by Number and Brightness Analysis. *Biophys. J.* **98**, 3078-3085 (2010).
13. Lajoie, P. & Snapp, E.L. Formation and Toxicity of Soluble Polyglutamine Oligomers in Living Cells. *PLoS ONE* **5**, e15245 (2011).
14. McKenna, B.K., Evans, J.G., Cheung, M.C. & Ehrlich, D.J. A parallel microfluidic flow cytometer for high-content screening. *Nat. Meth.* **8**, 401-403 (2011).
15. Rizzo, M.A., Springer, G.H., Granada, B. & Piston, D.W. An Improved Cyan Fluorescent Protein Variant Useful for FRET. *Nat Biotech* **22**, 445-449 (2004).
16. Olshina, M.A. et al. Tracking mutant huntingtin aggregation kinetics in cells reveals three major populations that include an invariant oligomer pool. *J. Biol. Chem.* **285**, 21807-21816 (2010).
17. Johannes, L., Tenza, D., Antony, C. & Goud, B. Retrograde transport of KDEL-bearing B-fragment of Shiga toxin. *J Biol Chem* **272**, 19554-19561 (1997).
18. Mallard, F. et al. Direct pathway from early/recycling endosomes to the Golgi apparatus revealed through the study of shiga toxin B-fragment transport. *J Cell Biol* **143**, 973-990 (1998).

List of supplementary items

Supplementary File	Title
Supplementary Fig. 1.	PulSA to distinguish cells with Htt_{ex1} inclusions compared to cells lacking Htt_{ex1} inclusions with two alternative approaches to GFP fusion.
Supplementary Fig. 2.	PulSA to detect suppressors and enhancers of inclusion formation.
Supplementary Fig. 3.	PulSA to track the behavior of SOD1 in Neuro2a cells
Supplementary Fig. 4.	Images of cells in suspension as prepared for flow cytometry.
Supplementary Fig. 5.	TC tags to monitor Htt conformation.
Supplementary Fig. 6.	Models for assembly of monomers into oligomers and inclusions in individual cells.
Supplementary Note 1.	Expanded discussion of aggregation models

EDITORIAL SUMMARY

By applying pulse shape analysis of flow cytometry data this work shows how protein localization changes can be monitored at high-throughput in cells. The authors use the technique in combination with tetracysteine-based oligomer sensors to monitor toxic protein aggregation in a cell model of Huntington's disease.

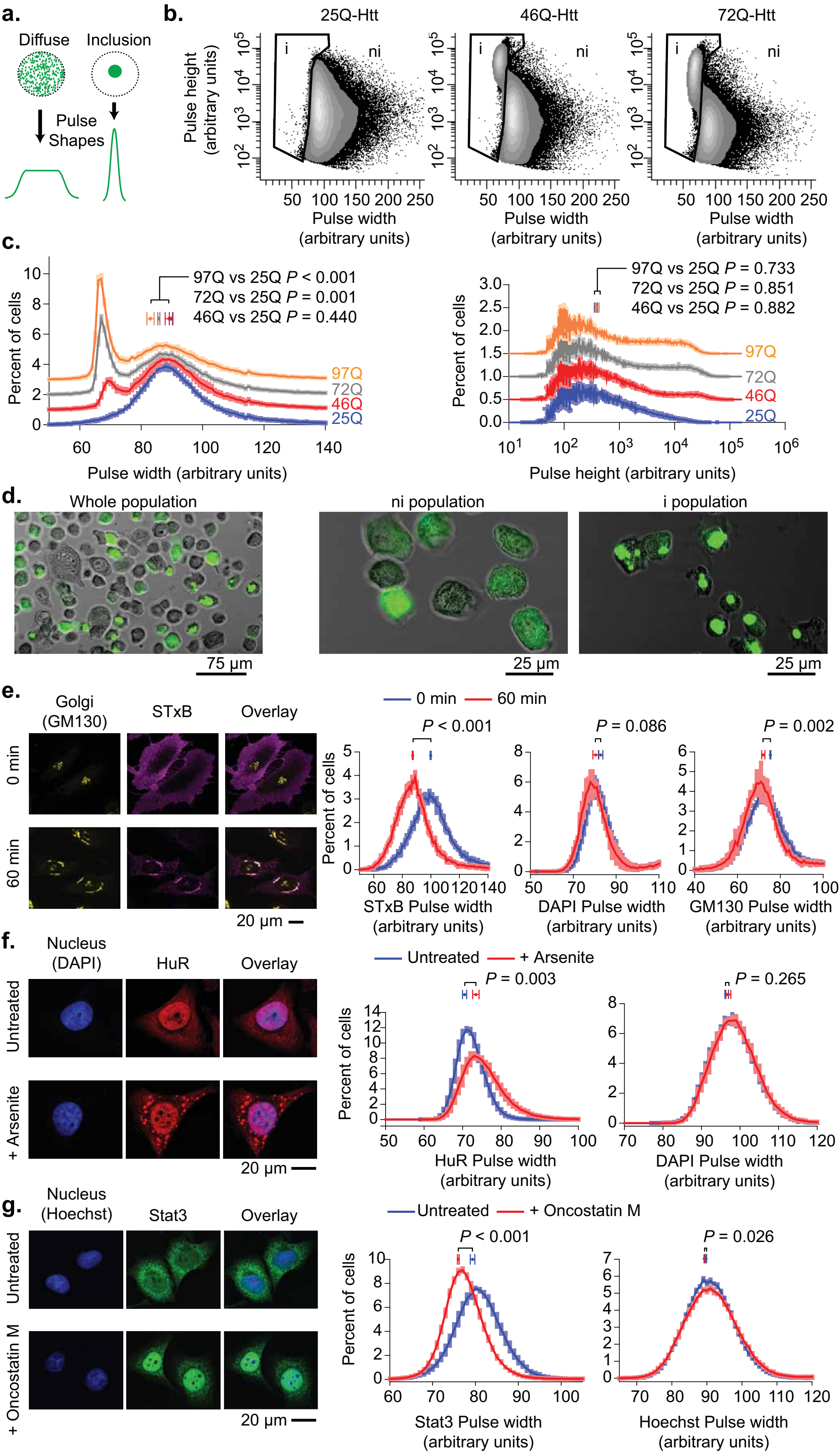
a.
Diffuse
Inclusion
Pulse Shapes
b.
25Q-Htt
46Q-Htt
72Q-Htt
Pulse height (arbitrary units)
i
ni
Pulse width (arbitrary units)
c.
Percent of cells
97Q vs 25Q P < 0.001
72Q vs 25Q P = 0.001
46Q vs 25Q P = 0.440
97Q
72Q
46Q
25Q
Pulse width (arbitrary units)
97Q vs 25Q P = 0.733
72Q vs 25Q P = 0.851
46Q vs 25Q P = 0.882
Pulse height (arbitrary units)
d.
Whole population
ni population
i population
75 µm
25 µm
e.
Golgi (GM130)
STxB
Overlay
0 min
60 min
20 µm
0 min
60 min
P < 0.001
P = 0.086
P = 0.002
STxB Pulse width (arbitrary units)
DAPI Pulse width (arbitrary units)
GM130 Pulse width (arbitrary units)
f.
Nucleus (DAPI)
HuR
Overlay
Untreated
+ Arsenite
20 µm
Untreated
+ Arsenite
P = 0.003
P = 0.265
HuR Pulse width (arbitrary units)
DAPI Pulse width (arbitrary units)
g.
Nucleus (Hoechst)
Stat3
Overlay
Untreated
+ Oncostatin M
20 µm
Untreated
+ Oncostatin M
P < 0.001
P = 0.026
Stat3 Pulse width (arbitrary units)
Hoechst Pulse width (arbitrary units)

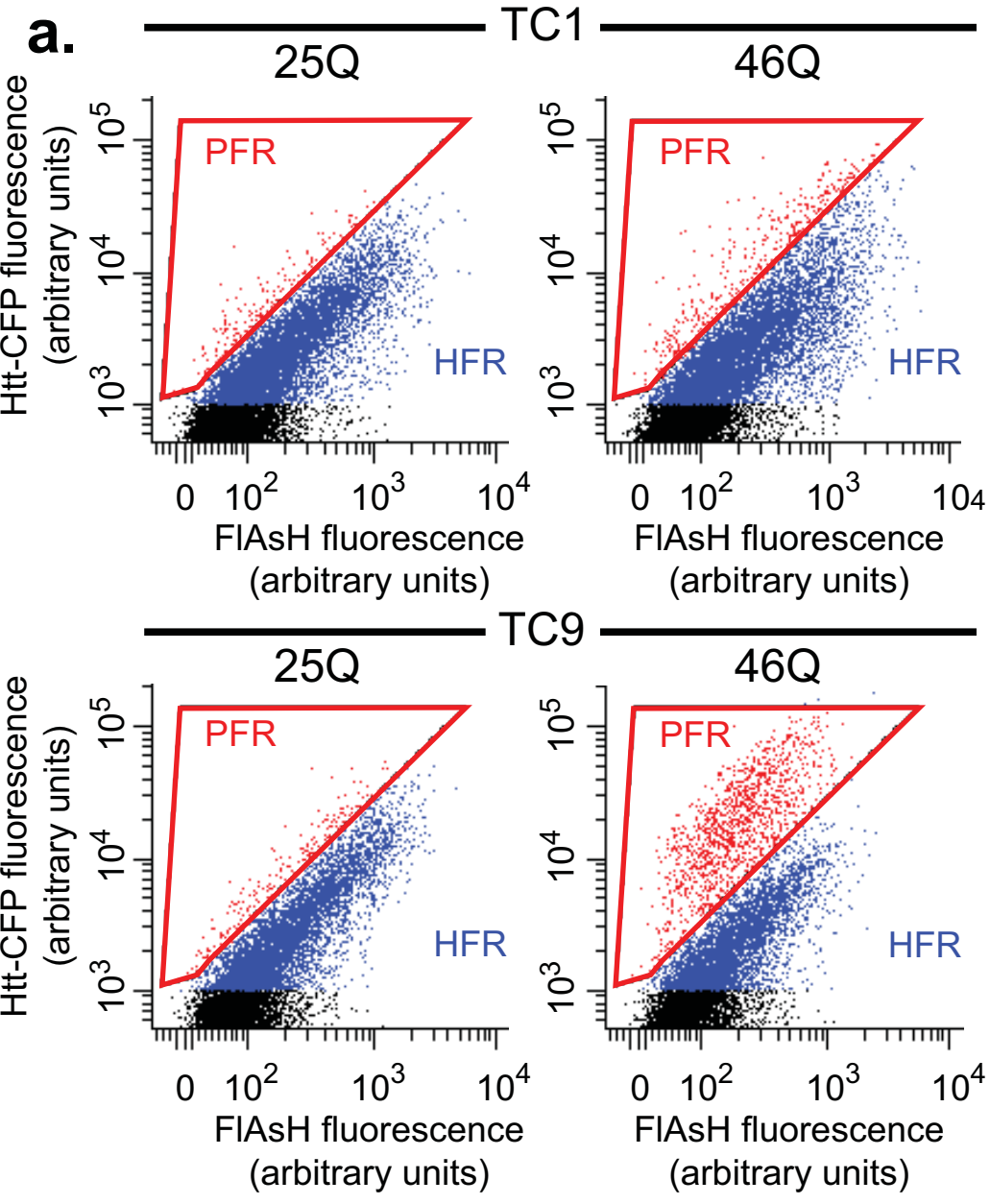
a.
TC1
25Q
46Q
PFR
HFR
Htt-CFP fluorescence (arbitrary units)
FlAsH fluorescence (arbitrary units)
TC9

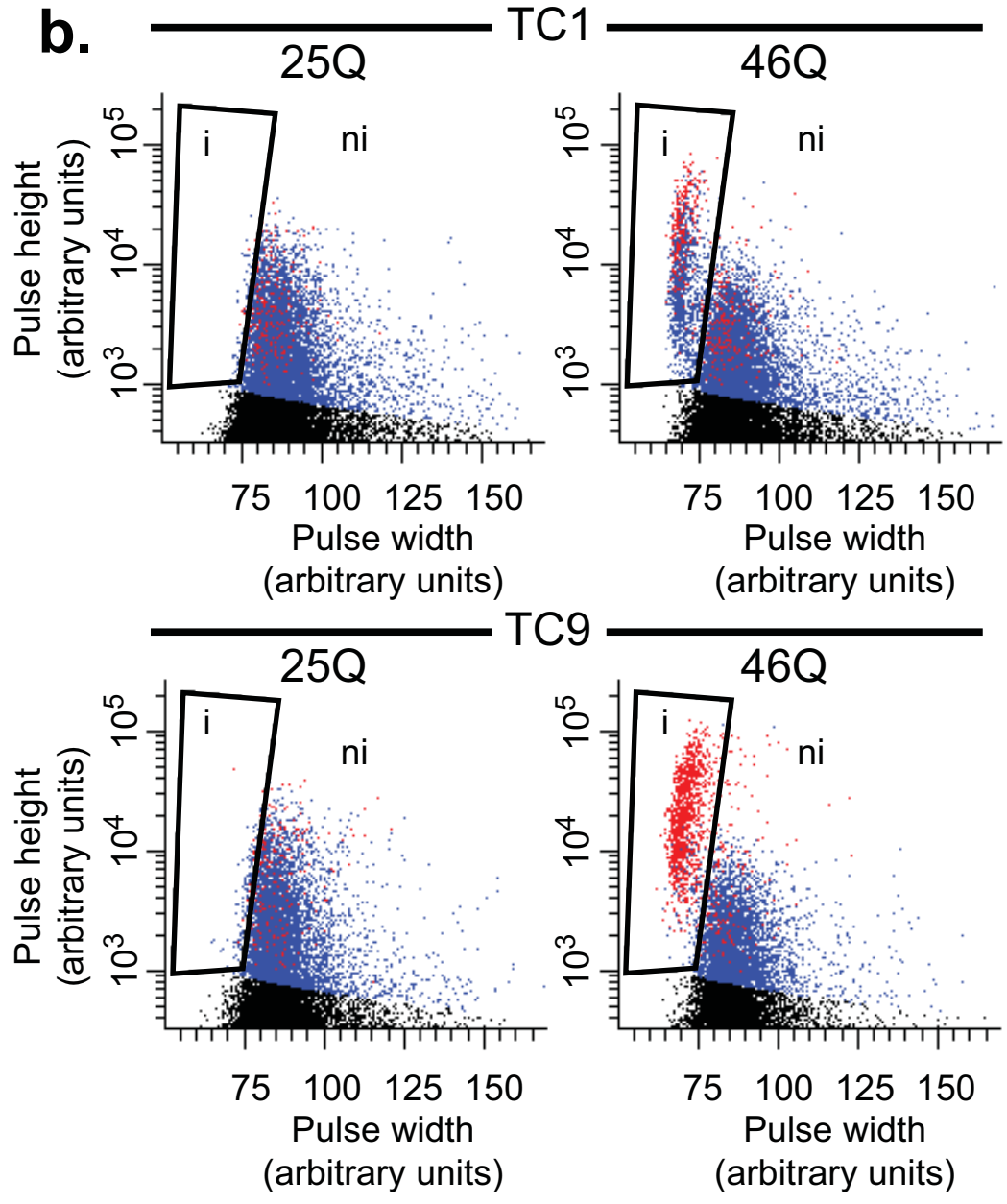
b.
TC1
25Q
46Q
i
ni
Pulse height (arbitrary units)
Pulse width (arbitrary units)
TC9

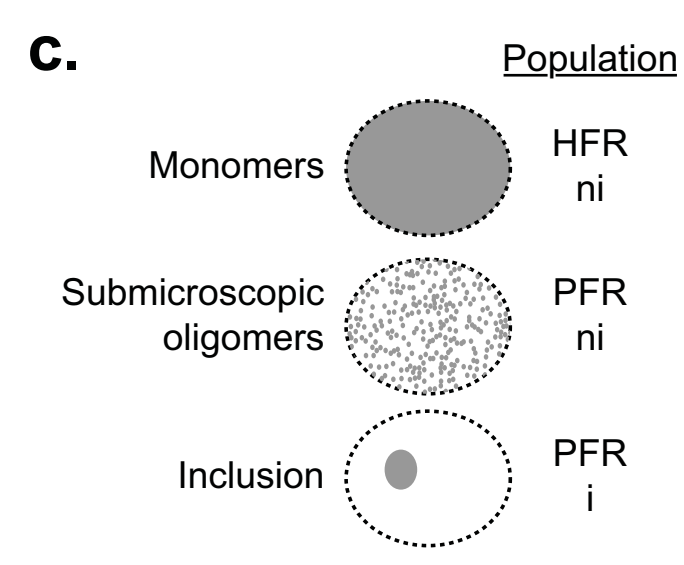
c.
Population
Monomers
HFR
ni
Submicroscopic oligomers
PFR
ni
Inclusion
PFR
i

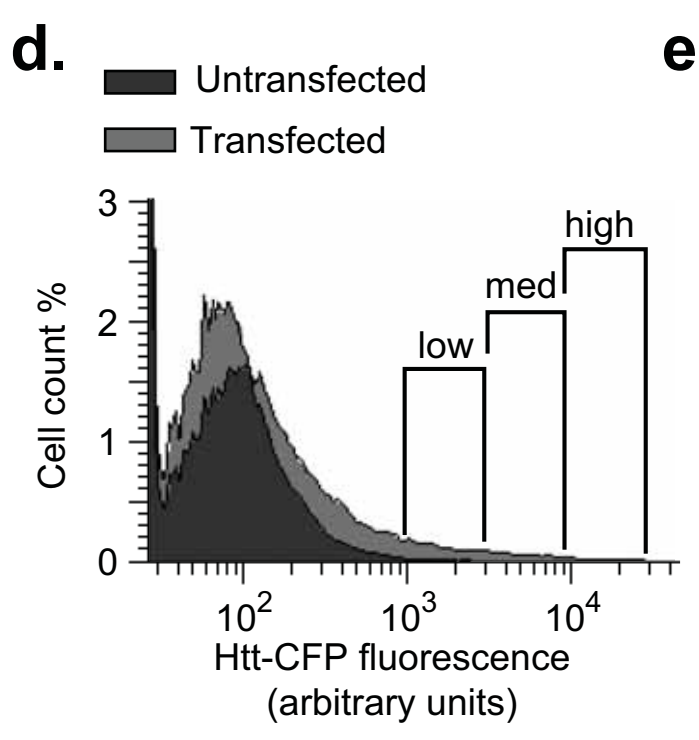
d.
Untransfected
Transfected
low
med
high
Cell count %
Htt-CFP fluorescence (arbitrary units)

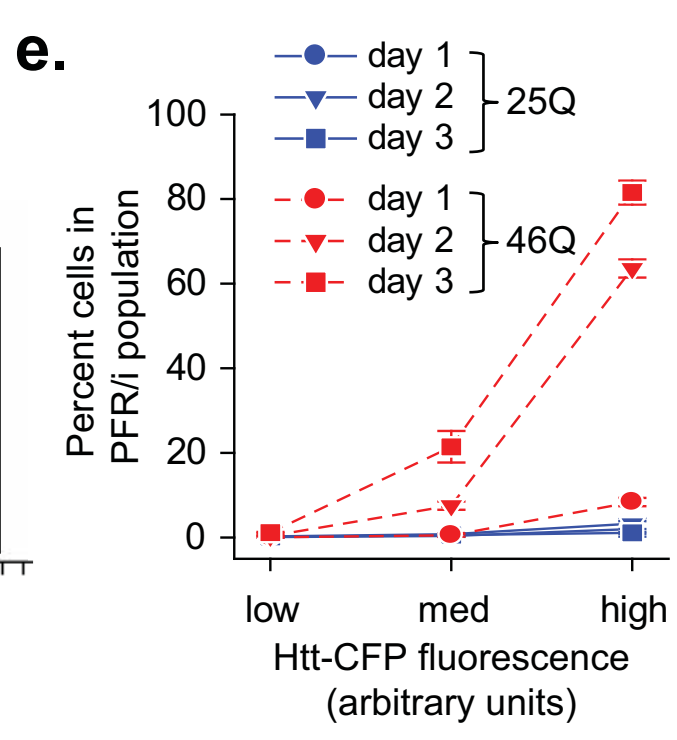
e.
day 1
day 2
day 3
25Q
46Q
Percent cells in PFR/i population
Htt-CFP fluorescence (arbitrary units)

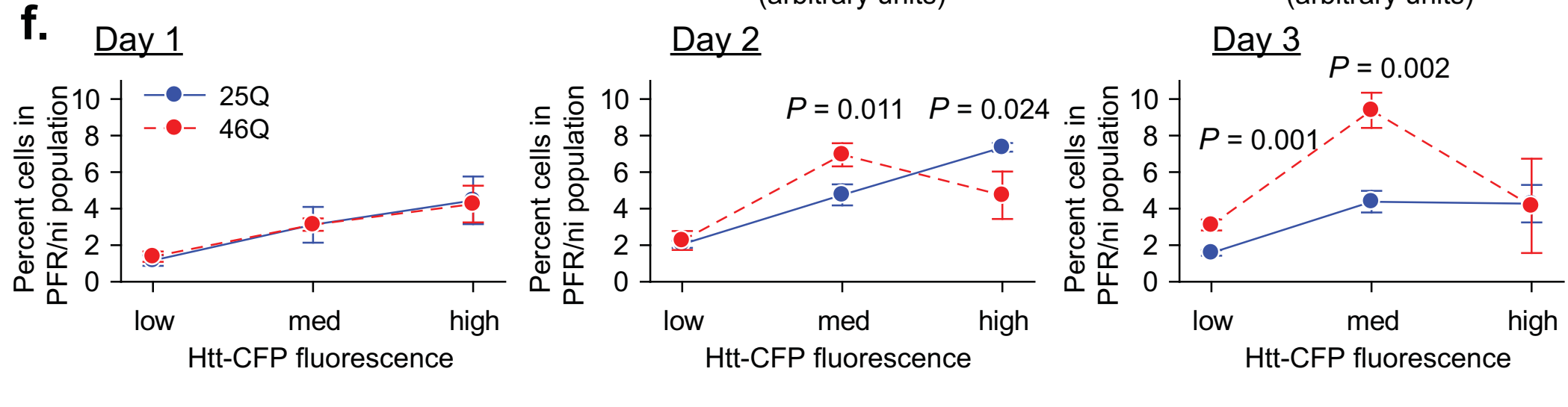
f.
Day 1
Day 2
Day 3
25Q
46Q
P = 0.011
P = 0.024
P = 0.001
P = 0.002
Percent cells in PFR/ni population
low
med
high
Htt-CFP fluorescence

Supplementary Figure 1. PulSA to distinguish cells with Htt_{ex1} inclusions compared to cells lacking Htt_{ex1} inclusions with two alternative approaches to GFP fusion.

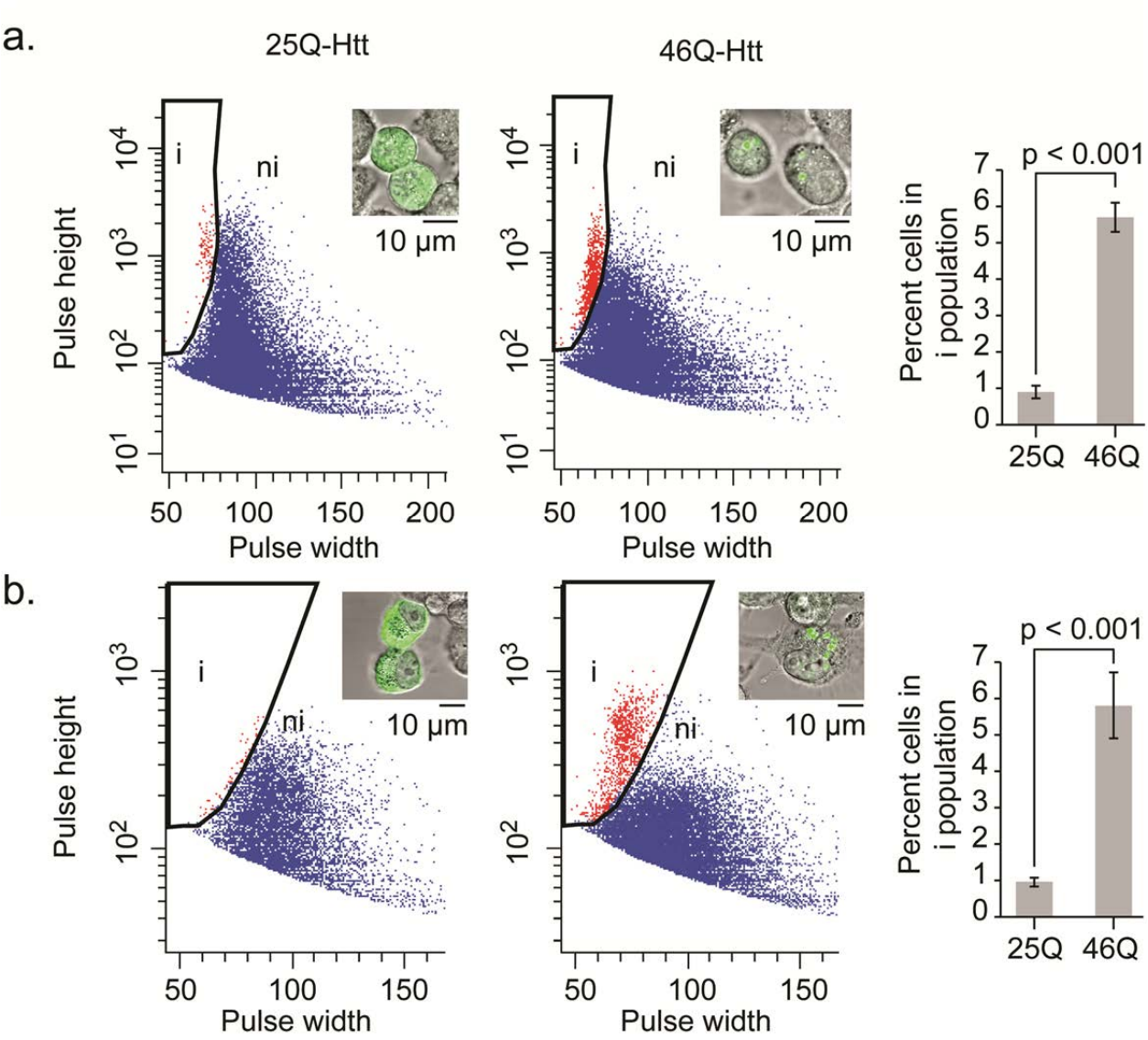

Htt_{ex1} was detected either with (**a**) a small tetracysteine (TC) motif to replace the GFP moiety, which can be fluorescently detected with the biarsenical dye FlAsH or (**b**) by immunodetection using the mEM48 anti-huntingtin antibody. Both approaches could be used to detect a specific i population in Neuro2a cells transfected with Htt_{ex1}. Quantification of i population (shown in red in cytograms) shows a significant number of cells with inclusions for the 46Q form of Htt_{ex1}. The differences between the 46Q and 25Q populations were evaluated by the Student's t-test (*n* = 3 independent experiments, mean ± s.d. shown).

Supplementary Figure 2. PulSA to detect suppressors and enhancers of inclusion formation.

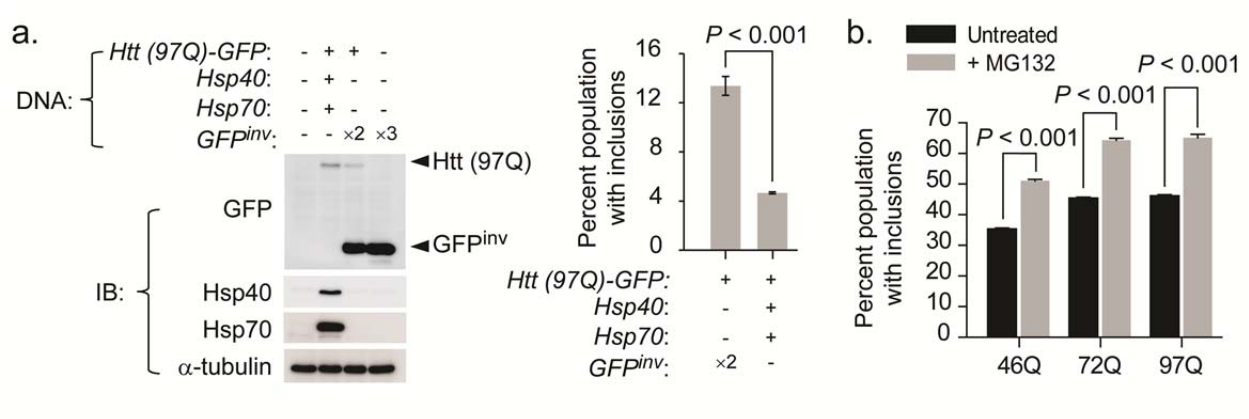

(**a**) Htt_{ex1}^{97Q}-Emerald was transfected into Neuro2a cells with equivalent amounts of DNA to match for total expression burden on cells. In this experiment, the total DNA used in the transfection was 4 µg and the Htt was kept at 1.33 µg. Each chaperone was added at 1.33 µg each and a non-fluorescent variant of GFP, GFP^{inv}, was added to bring the DNA up to 4 µg, as previously described [1]. PulSA of the cells expressing mutant Htt with or without Hsp40 and Hsp70 shows the chaperone overexpression to significantly reduce the number of cells with inclusions. The differences were evaluated by the Student's t-test (n = 3 independent experiments, mean ± s.d. shown). (**b**) Htt_{ex1}-Emerald constructs were transfected into HEK293 cells (4 µg) and assessed by PulSA 48 h post transfection with or without MG132 (50 µM) treatment, which significantly increases the number of cells with inclusions. The differences were evaluated by the Student's t-test (n = 3 independent experiments, mean ± s.d. shown).

Supplementary Figure 3. PulSA to track the behavior of SOD1 in Neuro2a cells.

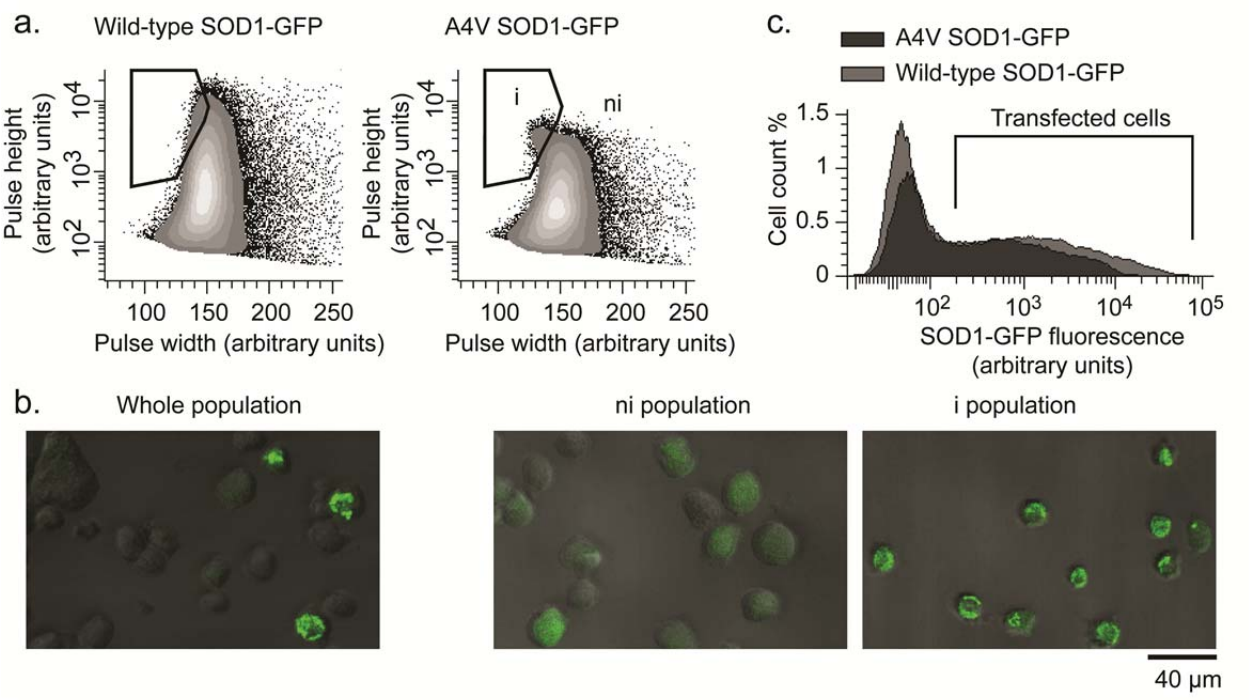

(**a**) Pulse shape analysis of SOD1-GFP reveals a new population, i, specific for a SOD1 mutant that induces it to progressively become mislocalized into puncta over time (A4V). (**b**) Separation of the i and ni populations for the A4V mutant SOD1 verifies that the i population contains mostly cells with abnormal SOD1 puncta, whereas the ni contains cells with normal, diffuse SOD1. (**c**) The A4V mutant causes a lower steady state level of expression, based on GFP fluorescence, in the highest expressing cells than the wild-type SOD1. An interesting feature of the data was that the i population of the A4V mutant overlapped with the ni population in the wild-type context and was less resolved than the corresponding Htt_{ex1} counterpart populations. This seems partly a result of lower expression levels of A4V SOD1-GFP relative to wild-type SOD1, which would disproportionately depress the number of cells at the higher pulse height values, and partly a result of the more diffuse inclusion morphology of SOD1 relative to inclusions of polyQ-expanded proteins [2]

Supplementary Figure 4. Images of cells in suspension as prepared for flow cytometry.

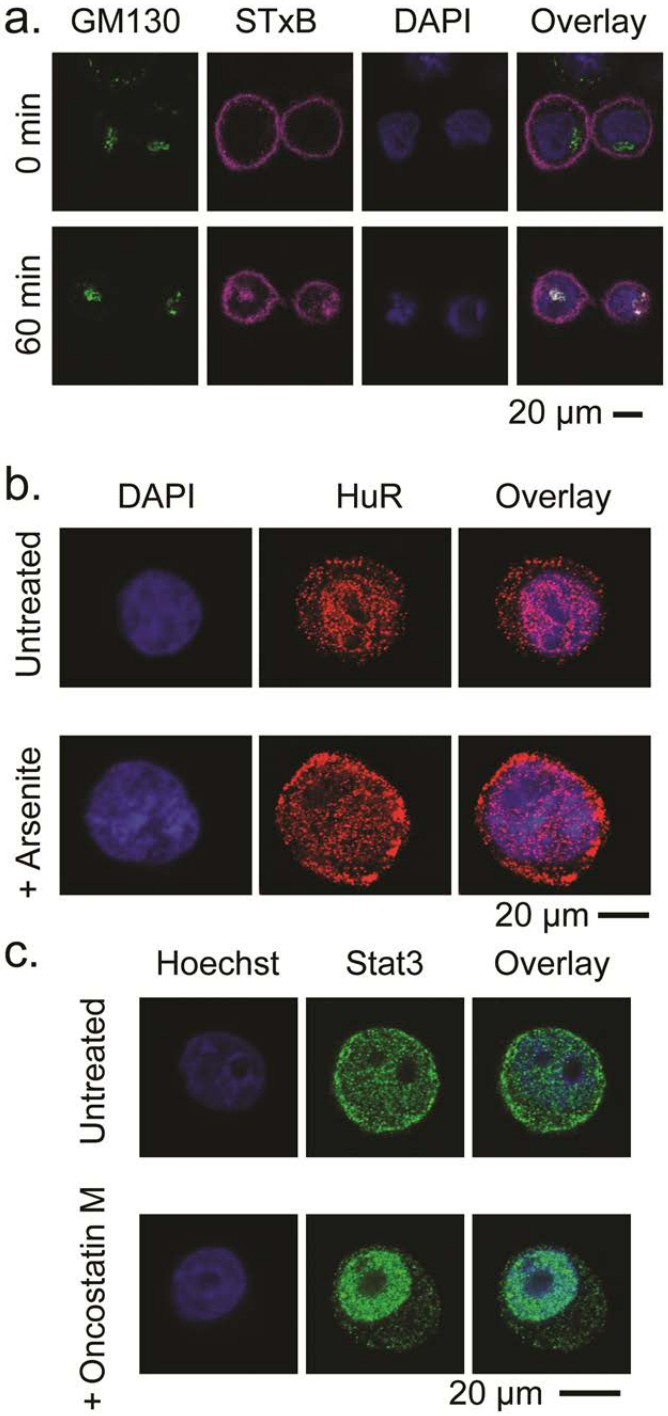

Panels (**a**), (**b)** and (**c)** correspond to the data collected in **Fig. 1d, e** and **f** respectively**.**

Supplementary Figure 5. TC tags to monitor Htt conformation.

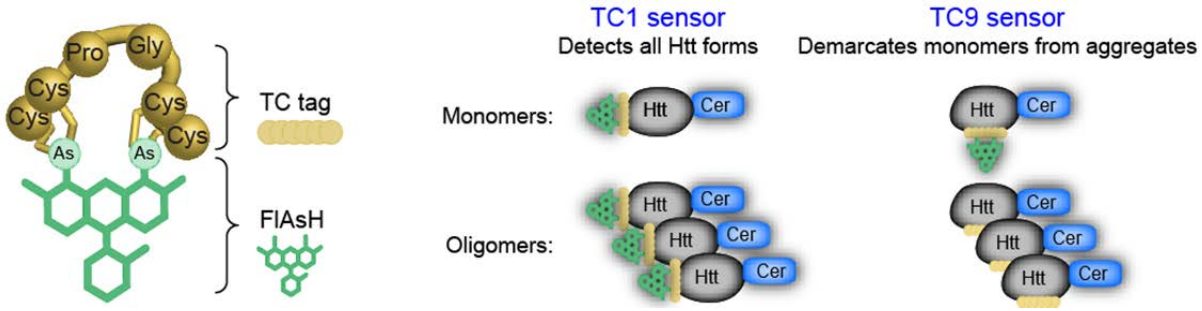

FlAsH is a fluorescein derivative containing two arsenic atoms (As) that bind four cysteines in the TC tag, as originally described [3]. In the TC1 sensor, a TC motif is located at the C-terminus of the exon 1 sequence of Htt, which enables efficient binding to FlAsH in monomers and oligomers [4]. In the TC9 sensor, the TC motif is located at the beginning of the polyQ sequence, which becomes occluded from binding FlAsH in oligomers

Supplementary Figure 6. Models for assembly of monomers into oligomers and inclusions in individual cells.

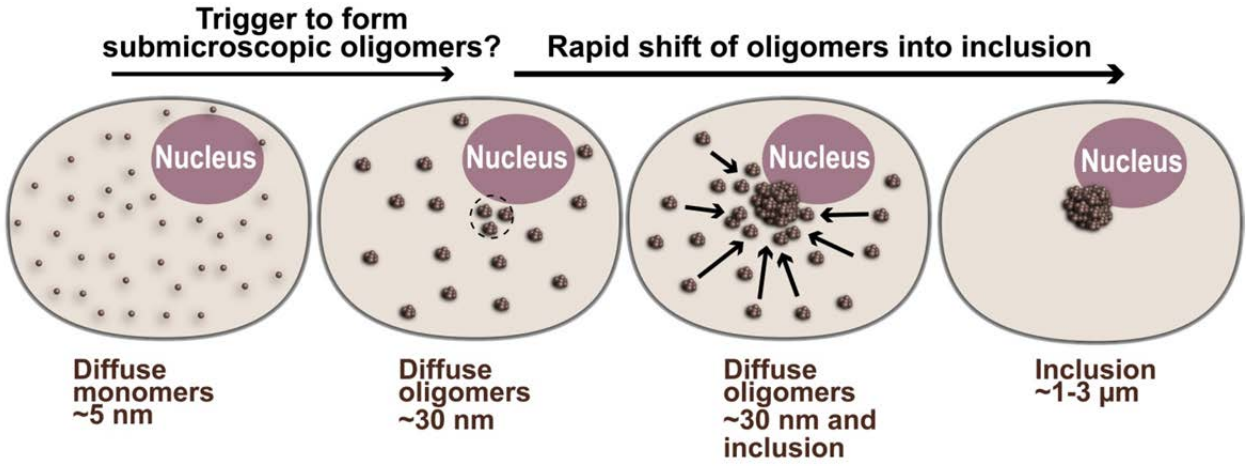

We propose monomers spontaneously self-assemble into nanometer sized toxic oligomers dispersed evenly through the cytosol. We and others have previously shown Htt_{ex1} forms oligomers that are approximately 30 nm in diameter [1, 5, 6]. Other work has shown that oligomers spontaneously form in cells once a critical monomer concentration threshold was reached [7]. We propose the formation of oligomers activates a rapid response from the cell to sequester oligomers into the inclusion, perhaps to detoxify them. Once inclusion formation begins, they have been reported to form in less than an hour and eventually sequester almost all the diffuse cytosolic Htt [7, 8].

Supplementary Note 1. Expanded discussion of aggregation models.

Our model is supported by previous studies suggesting that soluble oligomers correlate with toxicity and to precede the formation of an inclusion [9, 10]. Yet we cannot rule out the possibilities that monomers also can be directly recruited to the inclusion and that oligomers form as a parallel partition to inclusions or that there are different pools of oligomers reflecting multiple concurrent cellular engagements. Support for these modes of action come from studies showing chaperones can facilitate the formation of a parallel partition of soluble non-toxic polyQ aggregates, which could reflect a different quality control pathway driving distinct microaggregate entities [11, 12]. In addition, components of the quality control network, including chaperones [1, 13, 14], proteasome components [15] and cytoskeletal machinery [16] actively mediate the formation of inclusions suggesting a subpopulation of oligomers – perhaps the non-toxic ones – are "cargo" to inclusions or degradation mechanisms. Recent data also suggests that extended polyQ sequences can adopt unusually collapsed monomer conformations [17, 18], which combined with other data suggesting that a misfolded monomer is most toxic [19-21], raises the tantalizing possibility for cellular processes that drive misfolded monomers directly transferred to inclusions for sequestration, as has been recently proposed [22]. Our data in **Fig. 2**, also raises the possibility that the enrichment of oligomers is concentration dependent, whereby the shift of oligomers to inclusions occurs rapidly in cells with the highest expression levels, but may occur slowly (or not at all) in the lowest expressing cells. The enrichment of oligomers in cells with medium levels of protein expression could thus reflect an equilibrium in cellular mechanisms – those that promote inclusion formation and those that reflect distinct quality control processes such as those described above.

References

1. Olshina, M.A. et al. Tracking mutant huntingtin aggregation kinetics in cells reveals three major populations that include an invariant oligomer pool. *J. Biol. Chem.* **285**, 21807-21816 (2010).
2. Matsumoto, G., Kim, S. & Morimoto, R.I. Huntingtin and Mutant SOD1 Form Aggregate Structures with Distinct Molecular Properties in Human Cells. *J. Biol. Chem.* **281**, 4477-4485 (2006).
3. Griffin, B.A., Adams, S.R. & Tsien, R.Y. Specific Covalent Labeling of Recombinant Protein Molecules Inside Live Cells. *Science* **281**, 269-272 (1998).
4. Ramdzan, Y.M. et al. Conformation sensors that distinguish monomeric proteins from oligomers in live cells. *Chem. Biol.* **17**, 371-379 (2010).
5. Mukai, H. et al. Formation of Morphologically Similar Globular Aggregates From Diverse Aggregation-prone Proteins in Mammalian Cells. *Proc. Natl. Acad. Sci. USA* **102**, 10887-10892 (2005).
6. Legleiter, J. et al. Mutant Huntingtin fragments form oligomers in a polyglutamine length-dependent manner in vitro and in vivo. *J. Biol. Chem.* **285**, 14777-14790 (2010).
7. Ossato, G. et al. A Two-Step Path to Inclusion Formation of Huntingtin Peptides Revealed by Number and Brightness Analysis. *Biophys. J.* **98**, 3078-3085 (2010).
8. Gong, B., Lim, M.C.Y., Wanderer, J., Wyttenbach, A. & Morton, A.J. Time-lapse analysis of aggregate formation in an inducible PC12 cell model of Huntington's disease reveals time-dependent aggregate formation that transiently delays cell death. *Brain Res. Bull.* **75**, 146-157 (2008).
9. Takahashi, T. et al. Soluble Polyglutamine Oligomers Formed Prior to Inclusion Body Formation are Cytotoxic. *Hum. Mol. Genet.* **17**, 345-346 (2007).
10. Lajoie, P. & Snapp, E.L. Formation and Toxicity of Soluble Polyglutamine Oligomers in Living Cells. *PLoS ONE* **5**, e15245 (2011).
11. Behrends, C. et al. Chaperonin TRiC Promotes the Assembly of PolyQ Expansion Proteins into Nontoxic Oligomers. *Mol. Cell* **23**, 887-897 (2006).
12. Lotz, G.P. et al. Hsp70 and Hsp40 functionally interact with soluble mutant huntingtin oligomers in a classic ATP-dependent reaction cycle. *J. Biol. Chem.* **285**, 38183-38193 (2010).
13. Krobitsch, S. & Lindquist, S. Aggregation of Huntingtin in Yeast Varies with the Length of the Polyglutamine Expansion and the Expression of Chaperone Proteins. *Proc. Natl. Acad. Sci. USA* **97**, 1589-1594 (2000).
14. Zhang, X. & Qian, S.-B. Chaperone-mediated hierarchical control in targeting misfolded proteins to aggresomes. *Mol. Biol. Cell* **22**, 3277-3288 (2011).
15. Rousseau, E., Kojima, R., Hoffner, G., Djian, P. & Bertolotti, A. Misfolding of Proteins with a Polyglutamine Expansion Is Facilitated by Proteasomal Chaperones. *J. Biol. Chem.* **284**, 1917-1929 (2009).
16. Iwata, A., Riley, B.E., Johnston, J.A. & Kopito, R.R. HDAC6 and Microtubules Are Required for Autophagic Degradation of Aggregated Huntingtin. *J. Biol. Chem.* **280**, 40282-40292 (2005).
17. Walters, R.H. & Murphy, R.M. Examining Polyglutamine Peptide Length: A Connection between Collapsed Conformations and Increased Aggregation. *J. Mol. Biol.* **393**, 978-992 (2009).

18. Crick, S.L., Jayaraman, M., Frieden, C., Wetzel, R. & Pappu, R.V. Fluorescence Correlation Spectroscopy Shows That Monomeric Polyglutamine Molecules Form Collapsed Structures in Aqueous Solutions. *Proc. Natl. Acad. Sci. USA* **103**, 16764-16769 (2006).
19. Zhang, Q.C. et al. A Compact β Model of huntingtin Toxicity. *J. Biol. Chem.* **286**, 8188-8196 (2011).
20. Miller, J. et al. Identifying polyglutamine protein species in situ that best predict neurodegeneration. *Nat. Chem. Biol.* **7**, 925-934 (2011).
21. Nagai, Y. et al. A Toxic Monomeric Conformer of the Polyglutamine Protein. *Nat. Struct. Mol. Biol.* **14**, 332-340 (2007).
22. van Ham, T.J. et al. Identification of MOAG-4/SERF as a Regulator of Age-Related Proteotoxicity. *Cell* **142**, 601-612 (2010).